Fiber type effect on tribological behavior when cutting natural fiber reinforced plastics

F. Chegdani *, S. Mezghani, M. El Mansori, A. Mkaddem

Arts et Métiers ParisTech, MSMP Laboratory, Rue Saint Dominique, BP 508, 51006 Châlons-en-Champagne, Cedex, France

Keywords:
Natural fiber reinforced plastics
Profile milling process
Surface roughness
Multiscale process signature

A B S T R A C T

Recently, natural fiber reinforced plastic (NFRP) materials are becoming a viable alternative to synthetic fiber in many industrial applications which do not require high structural performances. However, machining of NFRP such as milling process is almost unavoidable operation to facilitate the parts assembly in addition to the finishing of final products. The present study thus focused on the influence of natural fiber types on tribological behavior during profile milling process. Three types of short natural fibers (bamboo, sisal and miscanthus) reinforced polypropylene (PP) composites are investigated. The quality of NFRP machined surface is quantified using a multiscale analysis based on wavelets decomposition. The natural fiber effects related to the machined surface quality is hence identified at all scales from roughness to waviness. The bamboo fibers reinforced plastics which exhibit high contact stiffness show the smoother surface finish after machining. Therefore, the multiscale surface roughness is used as descriptor of natural fiber influence on the machining mechanisms and to establish the cutting signature of NFRP materials.

1. Introduction

Fiber reinforced plastics are being more attractive in many engineering applications due to their higher mechanical properties compared to their low weights [1–5]. The use of natural fibers as plastic reinforcement has raised the interest of academia and industry from an economic and ecological point of view [6]. In addition to the low production cost, the use of natural fibers is justified by the valorization of local resources and the enhancement of materials and technologies taking into account the environmental impacts and the sustainable development [7].

Most of the composite manufacturing technologies generate some burrs at the edge of parts. Profile milling is an important machining step for deleting the extended burrs and achieving the dimensions of final products [8]. However, it is a complicated operation because of non-homogeneity in the internal structure of composite materials [9].

Several scientific studies have addressed the machining of synthetic fiber composites [10–16]. But a few works have been interested to the machining of natural fiber composites, especially the natural fiber reinforced plastics (NFRP). Previous works have been invested particularly in the drilling and milling operations in order to identify the overall variability behavior of NFRP during machining process in terms of surface roughness, cutting forces and delamination factor using statistical analysis of variance. These studies [17–26] show that the cutting feed rate has the larger effect on the cutting forces, delamination factor and surface roughness, followed by the tool diameter for drilling process and depth of cut in the case of milling operation. The cutting speed has the lowest contribution on the modification of the cut surface state. In fact, cutting forces, delamination factor and surface roughness increase with the increase of feed rate, tool diameter or the depth of cut.

Comparative studies between NFRP and glass fiber reinforced plastics (GFRP) show a clear difference in cutting behavior of these two materials [23,25]. The NFRP generate less cutting forces than GFRP during machining, but have more delamination induced-cutting damage with rough cut surfaces. Moreover, the local properties of fiber significantly influence the cutting behavior of NFRP in terms of delamination factor and surface roughness levels [19]. This is a sign that NFRP machining is very closely related to the fiber cutting. This is proven by the fact that the natural fiber intrinsic properties and structures are themselves a composite material of cellulose fibrils in a matrix of amorphous hemicellulose and lignin [27]. However, the physical reasons of the natural fiber effect on the differences in NFRP cutting behavior are still not yet understood. In fact, the cutting process in these studies was considered based on a systematic approach which has as input the process conditions (cutting speed, feed rate, depth of cut etc.) and as output the global surface roughness (R_a). The feedback of the R_a parameter is well known that is not relevant when machining composites materials [12,28,29].

* Corresponding author. Tel.: +33-326-69-91-59; fax: +33-326-96-91-97.
E-mail address: faissal.chegdani@ensam.eu (F. Chegdani).

Nomenclature

e	workpiece thickness (mm)
m_f	fiber mass fraction (wt%)
v_f	fiber volume fraction (vt%)
ρ_f	fiber density (g/cm^3)
ρ_c	composite density (g/cm^3)
E_f	fiber tensile modulus (GPa)
E_m	matrix tensile modulus (GPa)
E_c	composite tensile modulus (GPa)
σ_f	fiber yield strength (MPa)
σ_m	matrix yield strength (MPa)
σ_c	composite yield strength (MPa)
A	shape factor
l	fiber length (mm)
d	fiber diameter (μm)
ϕ_{max}	maximum packing fraction of the reinforcement
R_a	arithmetic mean deviation of roughness (ISO4287) (μm)
E_{sc}	specific cutting energy (J mm^{-3})
F_x	cutting force in the x direction (N)
F_y	cutting force in the y direction (N)
F_t	tangential cutting force (N)
D	milling tool diameter (mm)
V_c	cutting speed (m/min)
V_f	feed speed (mm/min)
f_z	tool feed rate (mm/tooth)
a	depth of cut (mm)
a_p	width of cut (mm)
P_c	cutting power (W)
Q	chip rate (mm^3/min)

In this paper, multiscale approach [30,31] was used to better understand the effect of fiber types when cutting NFRP materials. The tribo-energetic approach [32,33] was used to identify the activated mechanisms during the tribological cutting contacts in machining and then establish the relationship between the fiber properties and induced-cut surface state of NFRP.

2. Experimental procedure

2.1. Workpiece samples

Three different natural fibers are considered in this study (Fig. 1). Bamboo, sisal and miscanthus fiber are randomly oriented in workpiece samples and there lengths are about 1 mm. The samples are in the form of rectangular plates of 2 mm of thickness (Fig. 1(d)). The NFRP workpiece samples were provided by an industrial manufacturer[1] and are prepared by compounding and injection molding of polypropylene (PP) resin with the short randomly oriented fibers. Table 1 presents the optimal injection molding parameters used by the manufacturer to elaborate the studied NFRP. Table 2 presents the mechanical characteristics of NFRP used in this study.

Fiber volume fraction values are given by the manufacturer. Fiber mass fraction values are estimated by Eq. (1). Where m_f and v_f are the mass fraction and volume fraction, respectively. ρ_f and ρ_c are the fiber density and composite density, respectively. The three NFRP samples have equivalent values of fiber mass fraction.

Because of the high dispersion of natural fiber properties in the literature [1,35,37,38], the fiber tensile modulus and yield strength values of the studied natural fibers are estimated respectively from the tensile modulus and yield strength values of the NFRP composites (given in Table 2) by the rule of mixture of Halpin Tsai modified by Nielson and adapted for randomly discontinuous fiber composites [39,40] (Eqs. (2) and (3)). These estimated values are presented in Table 3 and are compared with the literature fiber tensile modulus values.

$$m_f = \frac{\rho_f}{\rho_c} v_f \tag{1}$$

$$E_f = \frac{(A+1)E_m}{1 - \dfrac{E_c - E_m}{v_f(\psi E_c + A E_m)}} \tag{2}$$

$$\sigma_f = \frac{(A+1)\sigma_m}{1 - \dfrac{\sigma_c - \sigma_m}{v_f(\psi \sigma_c + A \sigma_m)}} \tag{3}$$

where

$$\psi = 1 + \left(\frac{1 - \phi_{max}}{\phi_{max}^2} \right) v_f \tag{4}$$

In Eqs. (2) and (3), E_c, E_f and E_m are the modulus of the composite, fiber and matrix, respectively. σ_c, σ_f and σ_m are the yield strength of the composite, fiber and matrix, respectively. ϕ_{max} is the maximum packing fraction of the reinforcement. For random packing of fibers, $\phi_{max}=0.82$ [40]. $E_m=1240$ MPa and $\sigma_m=23$ MPa according to [41].

Finally, $A=2(l/d)$ where (l/d) is the fiber aspect ratio. Microscopic analyses were made in different parts of each NFRP composite to estimate the fiber length (l) and the fiber diameter (d). They show that the three studied natural fiber have the same mean length and diameter values. Indeed, $l=1$ mm and $d=200$ μm.

Each sample had its work-surface polished with the same grit size of sand paper before profile milling process in order to have the same initial surface state before machining surface analysis.

Geometrical and superficial variations of each workpiece samples have been measured at five locations using a 2D Surfascan stylus profilometer according to the *ISO*4287 standard. The tip radius of the diamond stylus is 2 μm. The surface micro-profile on each specimen was taken along the machining direction over a sampling length of 4 μm. The evaluation length is 16.8 mm and a cut-off of 0.8 mm is used to evaluate the arithmetic mean deviation of roughness (R_a) profile parameter. Each measurement has been performed before and after the profile milling test. Microscopic observations of surface state were made by a scanning electron microscope (SEM) at low vacuum mode (21 Pa).

3. Profile milling experiments

Profile milling tests were performed on instrumented DMU60 monoBLOCK® five axes CNC machine. Clamping system was mounted on a Kistler dynamometer in order to measure the cutting forces (F_x and F_y in Fig. 2 (b)). The milling tool chosen for this study is a helical carbide end mill of 12 mm of diameter and composed of two cutting edges with 25° of helix angle including polyglass flutes.

Tests have been realized on dry cutting contact conditions varying the feed of milling tool. All other working parameters are kept constant. Process parameters values are presented in Table 4.

[1] *See Acknowledgments section*

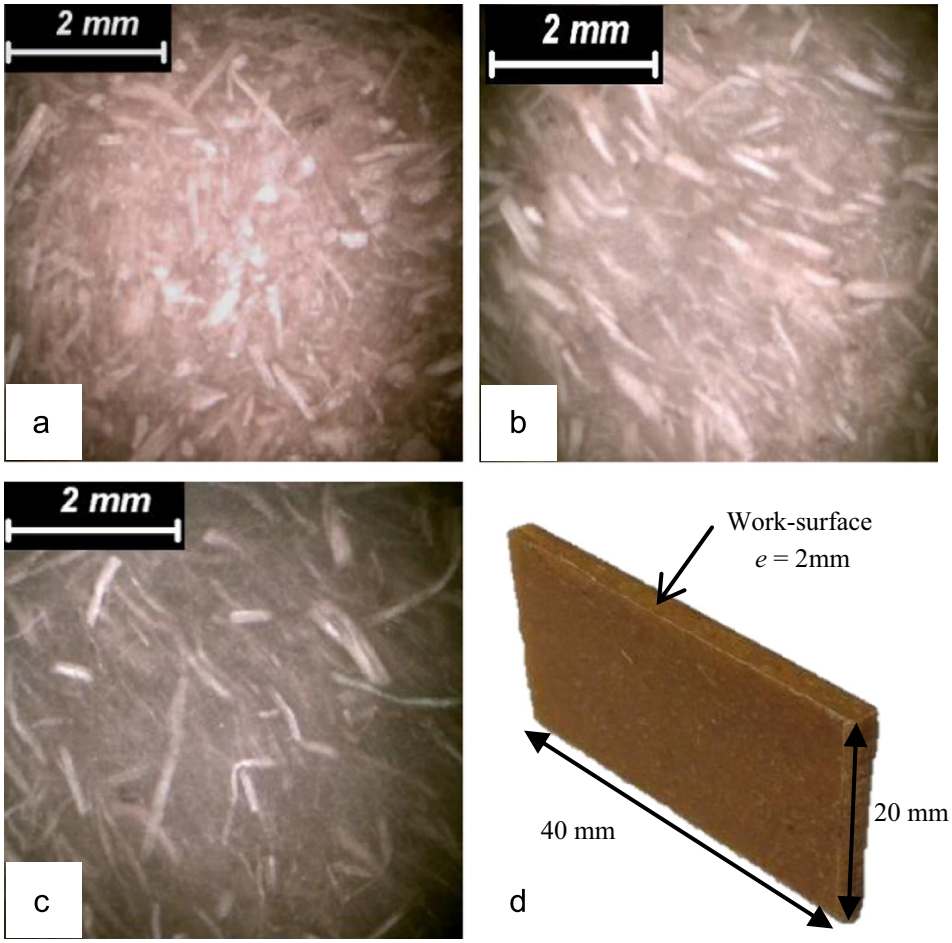

Fig. 1. Optical microscope pictures of each specimen of NFRP showing randomly oriented short fibers: (a) PP/bamboo, (b) PP/miscanthus, (c) PP/sisal, and (d) photograph of the workpiece sample showing the work surface.

Table 1
Injection molding parameters of studied NFRP samples.

	PP/bamboo	PP/miscanthus	PP/sisal
Melt flow rate (g/10 min)	10	30	7
Melt temperature		150–190 °C	
Hold-on pressure		50–70% of injection pressure	
Mold temperature		30–50 °C	
Drying		4 h at 100 °C	

Table 2
Mechanical characteristics of studied NFRP samples.

	PP/bamboo	PP/miscanthus	PP/sisal
Fiber volume fraction (%)	30	20	20
Composite density (g/cm^3)	1	0.98	0.95
Fiber density (g/cm^3) [34–36]	1.1	1.5	1.5
Fiber mass fraction (%)	33	30.6	31.6
Tensile modulus (GPa)	4.1	2.7	2.2
Yield strength (MPa)	40	30	28

4. Results and discussion

4.1. Microscopic surface finish observations

Fig. 3 compared SEM micrographs (surface states) of workpiece samples before and after profile milling operation. Initial state before machining shows polishing streaks and fiber debris. It also shows that the fiber cross sections appear composed by the gathering of several elementary fibers (Fig. 3(a), (c), (e)). However, sisal elementary fibers appear with more longitudinal and larger diameter.

Table 3
Estimated mechanical properties of natural fibers.

	Bamboo	Miscanthus	Sisal
Estimated fiber tensile modulus (GPa)	19	13.8	7.84
Estimated fiber yield strength (MPa)	89.2	62	50
Literature fiber modulus (GPa) [1,35,37,38]	11–32	4.5–60	8.4–38

After profile milling process, the studied natural fibers have different morphological aspects. This difference corresponds to the cutting signature of each NFRP material due to the activated mechanisms during profile milling operation. Bamboo fiber composite has smooth appearance at fiber bundle section in addition to some detached fiber zones (Fig. 3(b)). Fiber shearing is not perfect because fiber bundle cross sections morphology is not observable like initial state (Fig. 3(a)). For miscanthus fiber composite, the same aspect is observed in addition to fiber–fiber interface break in fiber bundle sections (Fig. 3(d)). However, sisal fiber composites clearly exhibit the fiber–fiber interface failure that causes the formation of some hollow spots (Fig. 3(f)). The sisal fiber extremities that exceed the machining surface are longer and more important than bamboo and miscanthus fiber ones.

SEM observations show that the natural fiber shearing mechanism is not purely ductile and its action is strongly depending on fiber type. This is due to the intrinsic mechanical properties of natural fibers and the adhesion properties between elementary

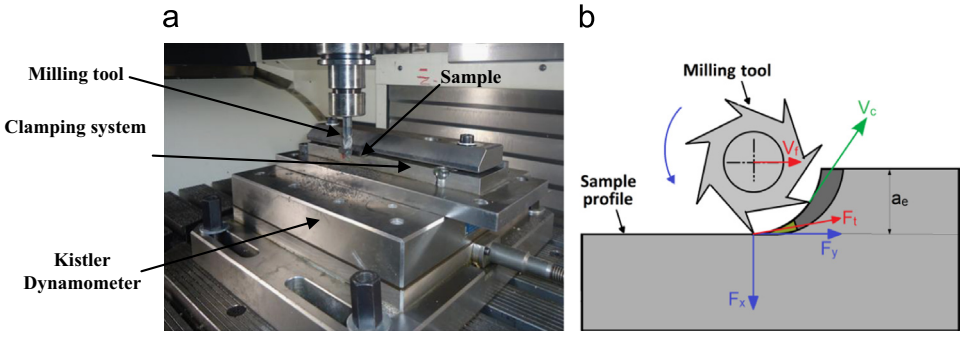

Fig. 2. (a) Experimental setup on five axes CNC machine. (b) Schema of profile milling process.

Table 4
Process parameters used in the profile milling tests.

Feed rate (mm/tooth)	Cutting speed (m/min)	Depth of cut (mm)
0.04 0.08 0.12	47	1

fibers themselves. Natural fibers are gathered in bundles of one to three dozen elementary fibers and the bundle cohesion is insured by pectin which have low mechanical properties [42]. Moreover, natural fibers are soft by nature due to their high cellulose content and this characteristic gives them the ability to deform under fiber–tool interaction [43]. Thus, in a contact between a rigid cutting tool and natural fiber, the energy can largely be dissipated through the deformation of the natural fiber. Then, the local deformation state of every area of the NFRP material when cutting (similar to viscoelastic material in contact with rough surface at extreme compressive and shear loading) is dependent on time and energy is dissipated by different mechanisms: friction, plowing and shearing. This may explain why the cutting process of NFRP is both a surface property (contact stiffness) and a volume property (internal behavior of natural fibers) since the cut surface of the fiber does not show a ductile regime (pure shearing).

5. Energetic analysis

Specific cutting energy has also been calculated from measured cutting forces in order to quantify the shearing mechanism contribution.

Specific cutting energy (E_{sc}) is obtained from cutting power (P_c) formula (Eq. (4)).

$$E_{sc} = \frac{P_c}{Q} \tag{4}$$

where Q is the chip rate defined by Eq. (5).

$$Q = a_p a_e V_f \tag{5}$$

where a_p, a_e and V_f are the width of cut, the depth of cut and the feed speed, respectively. Here, a_p corresponds to the sample thickness (i.e. $a_p = e = 2$ mm).

The cutting power is deducted from the cutting force, F_t (Eq. (6)):

$$P_c = F_t V_c \tag{6}$$

F_t presents the tangential component of cutting force in the local coordinate system (Fig. 2(b)) and its value is calculated from the measured cutting forces in global coordinate system (F_x and F_y) as described in [44]. It is important to note that specific cutting energy values for each material are normalized by the fiber volume fraction in order to obtain comparable results.

According to the estimated natural fiber stiffness values (Table 3) and the results of specific cutting energy (Fig. 4), the high stiffness of cutting contact makes the shearing of fibers easier, which is characterized by the lowest specific cutting energy. Fig. 4 (b) shows that high fiber stiffness decreases the specific cutting energy which means that high fiber stiffness leads to an easy fiber shearing when cutting NFRP. Bamboo fibers have the highest stiffness and present the easiest fiber shearing (Fig. 4(a)), but not enough to perform an ideal shearing during profile milling operation (Fig. 5(a)). Indeed, cutting operation is preceded by a small sliding between fibers and milling tool (due to the fiber deformation) before fibers shearing. Fiber extremities exceeding the machining surface still leaned in the feed direction (Fig. 5(b)). In addition, the low fiber–fiber adhesion [45] can lead to the break of the interfacial liaisons between elementary fibers during milling as observed on sisal NFRP and described in Fig. 5(c).

6. Workpieces surface finish

Fig. 6 shows an example of roughness profile of the different NFRP materials before and after machining process. The peaks correspond to the exceed fiber extremities of imperfect fiber shearing. The valleys correspond to the detached fiber zones or hollow spots caused by fiber–fiber interface break. It can be seen that sisal and miscanthus FRP roughness profile shows more irregularities than bamboo FRP roughness profile after milling.

In order to compare the finish surface state for the different materials, we calculated the global roughness gain ratio which was defined by [46]

$$\Delta R_a\ (\%) = \frac{R_a^{end} - R_a^{init}}{R_a^{init}} \times 100 \tag{7}$$

$R_a{}^{init}$ and R_a^{end} are respectively the surface roughness before and after profile milling process. Fig. 7 presents the results of global roughness gain ratio for the three studied materials.

Fig. 7 shows that, after profile milling process, the final roughness value can reach four times the initial roughness value in the case of sisal fibers. Bamboo and miscanthus seem to have the same behavior in terms of induced-machining roughness. Feed rate does not have a significant effect on global surface roughness gain ratio. The difference of global surface roughness between the natural fibers is consistent with SEM observations and energetic analysis. This comparison reveals that sisal fibers, which have the lowest cutting contact stiffness, are more contributing to the increase in surface roughness after machining because of the fiber extremities that exceed the machining surface (Fig. 5(b)).

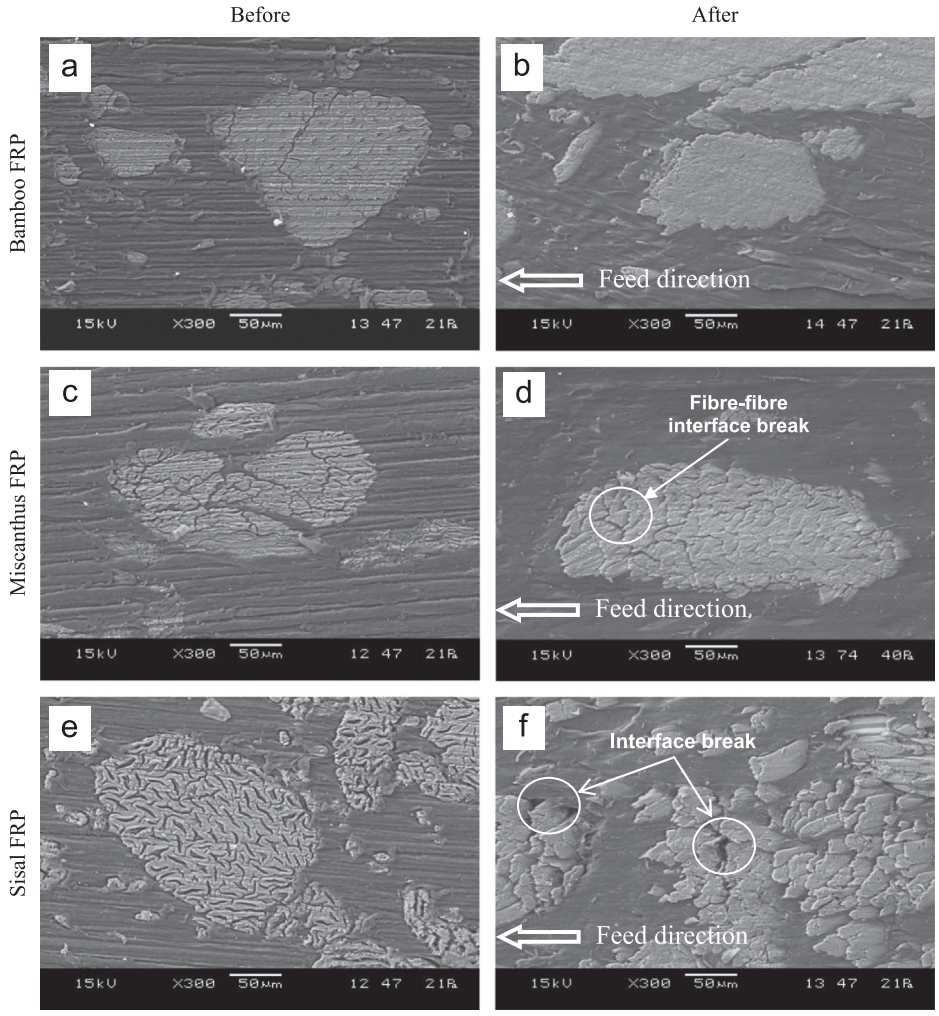

Fig. 3. SEM image of surface state of NFRP before and after profile milling process at f_z=0.04 mm/tooth.

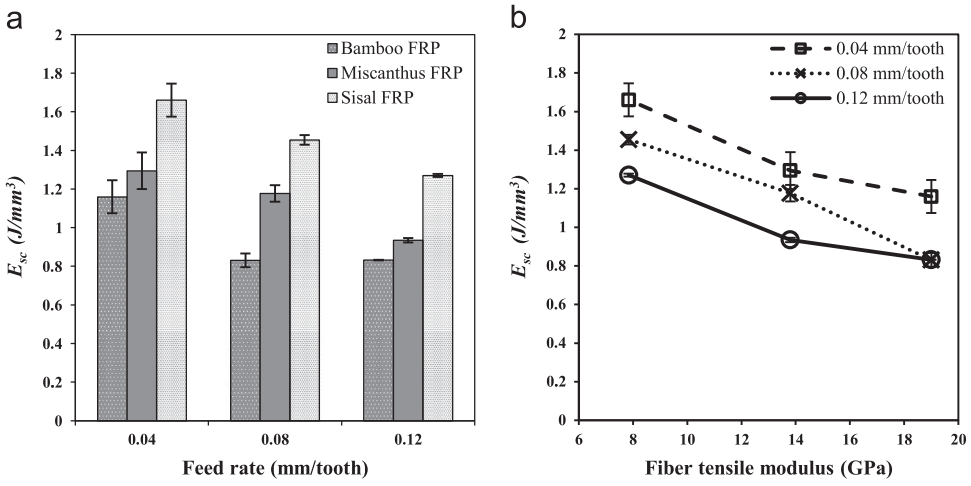

Fig. 4. (a) Specific cutting energy for each NFRP. (b) Relation between specific cutting energy and fiber tensile modulus.

7. Multiscale surface analysis

To correlate the cutting signature of NFRP with the cutting contact scale, we introduce a multiscale decomposition method of the surface topography based on Discrete Wavelets Transform (DWT) [47–49].

The DWT decomposes a signal into several sub-bands according to a recursive process. At each DWT decomposition, topographic signal $f(x)$ (Fig. 6) processed through a series of high-pass and low-pass filters to analyze the high and low frequencies [50]. The down-sampled output of the high-pass and low-pass filters are respectively the detail and approximate wavelets coefficients.

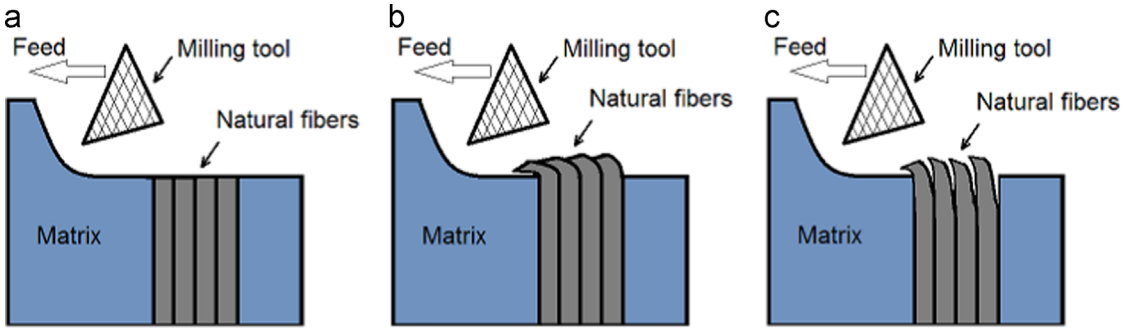

Fig. 5. Principal mechanisms when cutting NFRP. (a) Ideal shearing of fibers. (b) Real shearing of fibers. (c) Real shearing of fibers showing interfaces break.

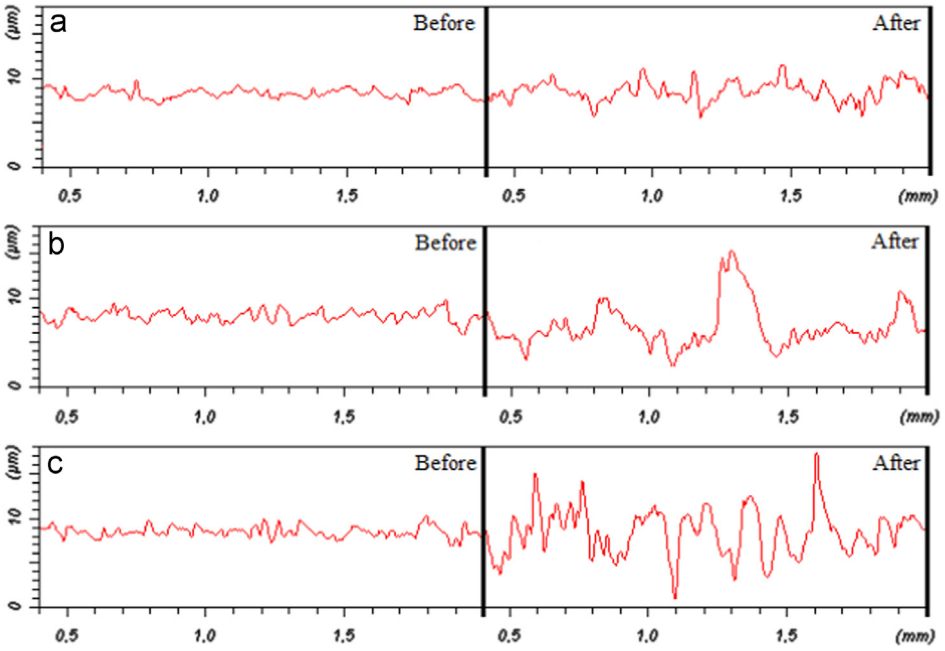

Fig. 6. Typical surface roughness pattern before and after profile milling process at f_z=0.04 mm/tooth. (a) bamboo FRP, (b) miscanthus FRP, and (c) sisal FRP.

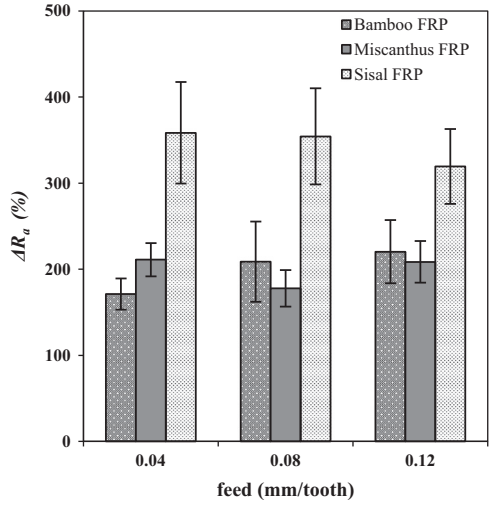

Fig. 7. Global roughness gain ratio for the three studied composite materials.

The procedure was then repeated for subsequent decompositions to achieve the desired level of the multi-resolution analysis. Then the wavelets coefficients were through synthesis filters to reconstruct the topographic signal at each decomposition levels.

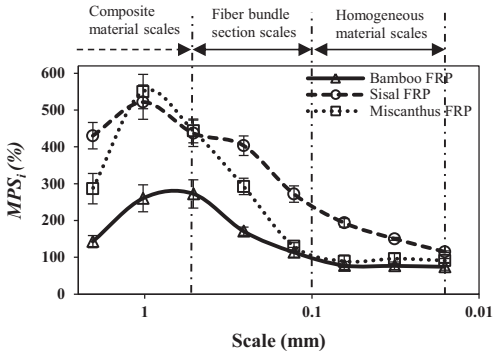

Fig. 8. Multiscale profile milling process signature for the different NFRP at f_z=0.04 mm/tooth.

Mathematically, a one dimension DWT is defined as follows [51]:

$$f(x) = \sum_{i,j} c_{i,j} \psi_{i,j}(x) \tag{8}$$

where $\psi_{i,j}(x)$ are the wavelet functions and and $c_{i,j}$ are the coefficients of $f(x)$. They are defined by

$$c_{i,j} = \int_{-\infty}^{+\infty} f(x) \psi_{i,j}(x) \tag{9}$$

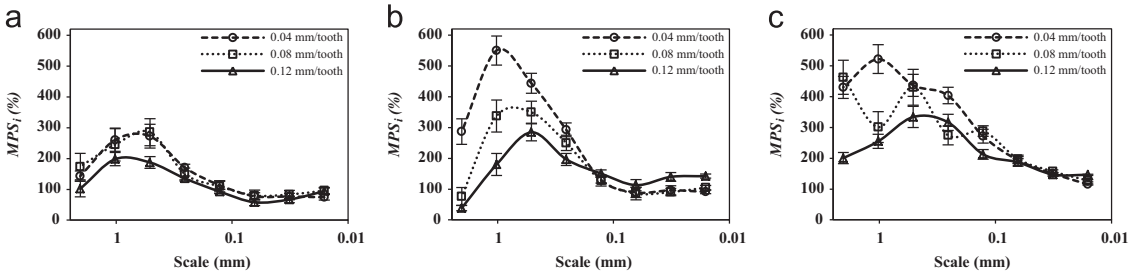

Fig. 9. Multiscale transfer function of profile milling process for the different values of feed rate. (a) Bamboo FRP, (b) miscanthus FRP, and (c) sisal FRP.

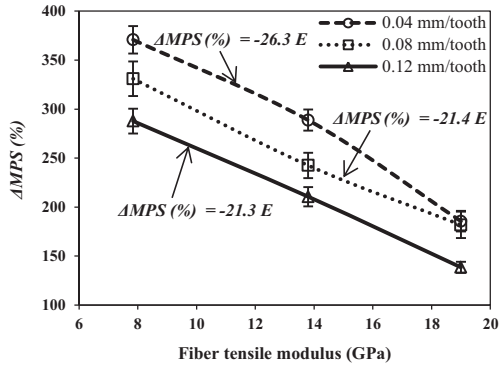

Fig. 10. Multiscale transfer function average vs tensile modulus at fiber bundle sections scales.

A mother wavelet $\psi_{i,j}(x)$ is used to generate the wavelet basis functions by using translation and dilation operations:

$$\psi_{i,j}(x) = 2^{-i/2}\psi(2^{-i}x - j) \tag{10}$$

where i and j are respectively the translation and dilation parameters.

The main advantages of the wavelet transform over the existing signal processing techniques are its space frequency localization and multi-scale analysis of roughness and waviness. This approach determines the multiscale transfer function of the morphological modification in surface topography after profile milling process denoted by multiscale process signature (MPS) [30].

The method consists in calculating the arithmetic mean roughness (M_a) on each decomposition scale "i" of the acquired roughness profile. multiscale profile milling process signature (MPS_i (%)) is obtained by calculating the ratio to the initial state of polishing (Eq. (11)).

$$MPS_i(\%) = \frac{M_a^{fin}(i) - M_a^{init}(i)}{M_a^{init}(i)} \times 100 \tag{11}$$

Fig. 8 shows that the surface roughness level is depending on measuring contact scale. For the three fiber types, the roughness is maximal at scale corresponding to the fiber size (~1 mm). The micro-roughness becomes quasi-constant at scales lower than 100 μm, which correspond to the elementary fiber cross section diameter. The fiber type impact on surface roughness is clearly identified at scales between 100 μm and 500 μm which correspond to the fiber bundle cross section diameters.

Fig. 9 reveals that the micro-roughness is independent of the feed rate (scales between 10 μm and 100 μm). The feed effect on profile milling surface roughness can be observed from 200 μm, which corresponds to the fiber bundle section scales and begins significant at composite scales. Miscanthus fiber composites are the most affected when increasing the feed rate. It shows that the feed increase contributes to the decrease of surface roughness ratio at fiber bundle section scales and composite scales. This exhibits that feed increase facilitates the fiber shearing during profile milling operation as it has been expressed by energetic analysis (Fig. 4), which shows that specific cutting energies decrease with feed.

Fig. 10 presents the relation between surface roughness and fiber stiffness. $\Delta MPS(\%)$ is the average of multiscale transfer function values at all fiber bundle section scales (between 100 and 500 μm). Tensile modulus values are obtained from the estimated mechanical properties of natural fibers (Table 3).

According to Fig. 10, the machining surface roughness of NFRP at fiber bundle section scales is almost linearly dependent on natural fiber stiffness. *MPS* function average is inversely proportional to the tensile modulus of natural fiber with a mean coefficient of approximately 23.

8. Conclusion

Multiscale milling process signature at NFRP fiber scales based on the wavelets transform has been determined to identify the impact of natural fibers on surface quality and cutting mechanisms. It makes possible to connect the surface topography modification to the mechanical properties of natural fibers. Then, multiscale topographic signature can be used as descriptor of natural fibers influence on profile machining mechanisms of NFRP. The results of this study provide the following conclusions:

- The cutting surface of NFRP is significantly dependent on fiber stiffness and interfaces quality.
- A viscoelastic behavior of natural fiber provokes an important fiber deformation and, then, an interfaces break during the contact with the milling tool. This generates an exceeded fiber extremities and debonding areas that contribute to the surface roughness increase.
- The effect of fiber type on milled surface roughness of NFRP is significantly obvious at fiber bundle cross section scales.
- Machining surface roughness decreases linearly with fiber stiffness at fiber bundle cross section scales.

Acknowledgments

The authors acknowledge the urban community of *Châlons-en-Champagne* (Cités en Champagne) for their financial support. The authors also wish to thank "*AD majoris SAS France*" for providing the NFRP samples used in this research.

References

[1] D.B. Dittenber, H.V.S. GangaRao, Critical review of recent publications on use of natural composites in infrastructure,, Compos. Part A Appl. Sci. Manuf. 43 (2012) 1419–1429. http://dx.doi.org/10.1016/j.compositesa.2011.11.019.

[2] O. Faruk, A.K. Bledzki, H.-P. Fink, M. Sain, Biocomposites reinforced with natural fibers: 2000–2010, Prog. Polym. Sci. 37 (2012) 1552–1596. http://dx.doi.org/10.1016/j.progpolymsci.2012.04.003.

[3] M. John, S. Thomas, Biofibres and biocomposites, Carbohydr. Polym. 71 (2008) 343–364. http://dx.doi.org/10.1016/j.carbpol.2007.05.040.

[4] D.U. Shah, Developing plant fibre composites for structural applications by optimising composite parameters: a critical review, J. Mater. Sci. 48 (2013) 6083–6107. http://dx.doi.org/10.1007/s10853-013-7458-7.

[5] P. Wambua, J. Ivens, I. Verpoest, Natural fibres: can they replace glass in fibre reinforced plastics? Compos. Sci. Technol. 63 (2003) 1259–1264. http://dx.doi.org/10.1016/S0266-3538(03)00096-4.

[6] A. Shalwan, B.F. Yousif, In state of art: mechanical and tribological behavior of polymeric composites based on natural fibres, Mater. Des. 48 (2013) 14–24. http://dx.doi.org/10.1016/j.matdes.2012.07.014.

[7] A. Lefeuvre, A. Bourmaud, C. Morvan, C. Baley, Tensile properties of elementary fibres of flax and glass: analysis of reproducibility and scattering, Mater. Lett. 130 (2014) 289–291. http://dx.doi.org/10.1016/j.matlet.2014.05.115.

[8] J.P. Davim, P. Reis, Damage and dimensional precision on milling carbon fiber-reinforced plastics using design experiments, J. Mater. Process. Technol. 160 (2005) 160–167. http://dx.doi.org/10.1016/j.jmatprotec.2004.06.003.

[9] S. Abrate, D. Walton, Machining of composite materials. Part II: non-traditional methods, Compos. Manuf. 3 (1992) 85–94. http://dx.doi.org/10.1016/0956-7143(92)90120-J.

[10] R. Zitoune, F. Collombet, F. Lachaud, R. Piquet, P. Pasquet, Experiment-calculation comparison of the cutting conditions representative of the long fiber composite drilling phase, Compos. Sci. Technol. 65 (2005) 455–466. http://dx.doi.org/10.1016/j.compscitech.2004.09.028.

[11] A. Ben Soussia, A. Mkaddem, M. El Mansori, Rigorous treatment of dry cutting of FRP–interface consumption concept: a review, Int. J. Mech. Sci. 83 (2014) 1–29. http://dx.doi.org/10.1016/j.ijmecsci.2014.03.017.

[12] P. Ghidossi, M. El Mansori, F. Pierron, Influence of specimen preparation by machining on the failure of polymer matrix off-axis tensile coupons, Compos. Sci. Technol. 66 (2006) 1857–1872. http://dx.doi.org/10.1016/j.compscitech.2005.10.009.

[13] P. Ghidossi, M. El Mansori, F. Pierron, Edge machining effects on the failure of polymer matrix composite coupons,, Compos. Part A Appl. Sci. Manuf. 35 (2004) 989–999. http://dx.doi.org/10.1016/j.compositesa.2004.01.015.

[14] L. Larbi, M. Nouari, M. El Mansori, Working parameters effects on machining-induced damage of fibre-reinforced composites: numerical simulation analysis, Int. J. Mater. Prod. Technol. 32 (2008) 136. http://dx.doi.org/10.1504/IJMPT.2008.018977.

[15] C.R. Dandekar, Y.C. Shin, Modeling of machining of composite materials: a review, Int. J. Mach. Tools Manuf. 57 (2012) 102–121. http://dx.doi.org/10.1016/j.ijmachtools.2012.01.006.

[16] A. Mkaddem, A. Ben Soussia, M. El Mansori, Wear resistance of CVD and PVD multilayer coatings when dry cutting fiber reinforced polymers (FRP), Wear 302 (2013) 946–954. http://dx.doi.org/10.1016/j.wear.2013.03.017.

[17] S.A.S. Azuan, Effects of drilling parameters on delamination of coconut meat husk reinforced polyester composites, Adv. Environ. Biol 7 (2013) 1097–1100.

[18] D. Babu, S. Babu, B.U.M. Gowd, Effects of machinig parameters in the drilling of jute fiber reinforced plastic: evaluation of the delamination factor, Glob. J. Mech. Eng. Comput. Sci. 2 (2012) 57–62.

[19] G.D. Babu, K.S. Babu, B.U.M. Gowd, Effect of machining parameters on milled natural fiber-reinforced plastic composites, J. Adv. Mech. Eng. 1 (2013) 1–12. http://dx.doi.org/10.7726/jame.2013.1001.

[20] G.D. Babu, K.S. Babu, B.U.M. Gowd, Effects of drilling parameters on delamination of hemp fiber reinforced composites, Int. J. Mech. Eng. Res. Dev. 2 (2012) 1–8.

[21] P.K. Bajpai, I. Singh, Drilling behavior of sisal fiber-reinforced polypropylene composite laminates,, J. Reinf. Plast. Compos. 32 (2013) 1569–1576. http://dx.doi.org/10.1177/0731684413492866.

[22] D. Chandramohan, K. Marimuthu, Drilling of natural fiber particle reinforced polymer composite material, Int. J. Adv. Eng. Res. Stud. 1 (2011) 134–145.

[23] L.M.P. Durão, D.J.S. Gonçalves, J.M.R.S. Tavares, V.H.C. de Albuquerque, T.H. Panzera, L.J. Silva, et al., Drilling delamination outcomes on glass and sisal reinforced plastics, Mater. Sci. Forum 730–732 (2012) 301–306. http://dx.doi.org/10.4028/www.scientific.net/MSF.730-732.301.

[24] S. Jayabal, U. Natarajan, Drilling analysis of coir-fibre-reinforced polyester composites, Bull. Mater. Sci. 34 (2011) 1563–1567. http://dx.doi.org/10.1007/s12034-011-0359-y.

[25] P.N.E. Naveen, M. Yasaswi, R.V. Prasad, Experimental investigation of drilling parameters on composite materials, J. Mech. Civ. Eng. 2 (2012) 30–37.

[26] R.N. Vinayagamoorthy, Analysis of cutting forces during milling of natural fibered composites using fuzzy logic, Int. J. Compos. Mater. Manuf. 2 (2012) 15–21.

[27] C. Baley, Analysis of the flax fibres tensile behavior and analysis of the tensile stiffness increase, Compos.—Part A Appl. Sci. Manuf. 33 (2002) 939–948. http://dx.doi.org/10.1016/S1359-835X(02)00040-4.

[28] D.H. Wang, M. Ramulu, D. Arola, Orthogonal cutting mechanisms of graphite/epoxy composite. Part I: unidirectional laminate, Int. J. Mach. Tools Manuf. 35 (1995) 1623–1638. http://dx.doi.org/10.1016/0890-6955(95)00014-O.

[29] Y. Landon, M. Cherif, Characterization of the surface quality of holes drilled in CFRP laminates (accessed 26.11.14), Adv. Mater. Res. 698 (2013) 107–116 ⟨http://www.scientific.net/AMR.698.107⟩.

[30] S. Mezghani, M. El Mansori, A. Massaq, P. Ghidossi, Correlation between surface topography and tribological mechanisms of the belt-finishing process using multiscale finishing process signature, C. R. Méc. 336 (2008) 794–799. http://dx.doi.org/10.1016/j.crme.2008.09.002.

[31] M. El Mansori, S. Mezghani, L. Sabri, H. Zahouani, On concept of process signature in analysis of multistage surface formation, Surf. Eng. 26 (2010) 216–223. http://dx.doi.org/10.1179/174329409X455412.

[32] E. Sura, M. El Mansori, P. Ghidossi, S. Deblaise, T.D. Negro, H. Khanfir, An energy analysis of belt polishing process and its applications to time cycle and tracking effects, Mach. Sci. Technol. 11 (2007) 217–234. http://dx.doi.org/10.1080/10910340701340059.

[33] H.A. Abdel-Aal, M. Nouari, M. El Mansori, Tribo-energetic correlation of tool thermal properties to wear of WC-Co inserts in high speed dry machining of aeronautical grade titanium alloys, Wear 266 (2009) 432–443. http://dx.doi.org/10.1016/j.wear.2008.04.023.

[34] K.J. Wong, S. Zahi, K.O. Low, C.C. Lim, Fracture characterisation of short bamboo fibre reinforced polyester composites, Mater. Des. 31 (2010) 4147–4154. http://dx.doi.org/10.1016/j.matdes.2010.04.029.

[35] L. Lundquist, G. Arpin, Y. Leterrier, F. Berthold, M. Lindström, J.-A.E. Manson, Alkali–methanol–anthraquinone pulping of *Miscanthus* × *giganteus* for thermoplastic composite reinforcement, J. Appl. Polym. Sci. 92 (2004) 2132–2143. http://dx.doi.org/10.1002/app.20179.

[36] R.W. Truss, Natural fibers for biocomposites, MRS Bull. 36 (2011) 711–715. http://dx.doi.org/10.1557/mrs.2011.207.

[37] K. Kaack, K.-U. Schwarz, Morphological and mechanical properties of Miscanthus in relation to harvesting, lodging, and growth conditions, Ind. Crops Prod. 14 (2001) 145–154. http://dx.doi.org/10.1016/S0926-6690(01)00078-4.

[38] F.D.A. Silva, N. Chawla, R.D.D.T. Filho, Tensile behavior of high performance natural (sisal) fibers, Compos. Sci. Technol. 68 (2008) 3438–3443. http://dx.doi.org/10.1016/j.compscitech.2008.10.001.

[39] L.E. Nielsen, Mechanical Properties of Polymer and Composites, Marcel Dekker Inc., New York, 1974.

[40] Y. Lu, Mechanical Properties of Random Discontinuous Fiber Composites Manufactured from the Wetlay Process, Master's thesis, Virginia Polytechnic Institute and State University, Blacksburg, 2002 ⟨http://scholar.lib.vt.edu/theses/available/etd-08132002-163349/⟩.

[41] R. Strapasson, S.C. Amico, M.F.R. Pereira, T.H.D. Sydenstricker, Tensile and impact behavior of polypropylene/low density polyethylene blends, Polym. Test. 24 (2005) 468–473. http://dx.doi.org/10.1016/j.polymertesting.2005.01.001.

[42] C. Morvan, C. Andème-Onzighi, R. Girault, D.S. Himmelsbach, A. Driouich, D.E. Akin, Building flax fibres: more than one brick in the walls, Plant Physiol. Biochem. 41 (2003) 935–944. http://dx.doi.org/10.1016/j.plaphy.2003.07.001.

[43] U. Nirmal, K.O. Low, J. Hashim, On the effect of abrasiveness to process equipment using betelnut and glass fibres reinforced polyester composites, Wear 290–291 (2012) 32–40. http://dx.doi.org/10.1016/j.wear.2012.05.022.

[44] D. Kalla, J. Sheikh-Ahmad, J. Twomey, Prediction of cutting forces in helical end milling fiber reinforced polymers, Int. J. Mach. Tools Manuf. 50 (2010) 882–891. http://dx.doi.org/10.1016/j.ijmachtools.2010.06.005.

[45] K. Charlet, A. Béakou, Mechanical properties of interfaces within a flax bundle – Part I: experimental analysis, Int. J. Adhes. Adhes. 31 (2011) 875–881. http://dx.doi.org/10.1016/j.ijadhadh.2011.08.008.

[46] S. Mezghani, M. El Mansori, E. Sura, Wear mechanism maps for the belt finishing of steel and cast iron, Wear 267 (2009) 86–91. http://dx.doi.org/10.1016/j.wear.2008.12.113.

[47] H. Zahouani, S. Mezghani, C. Pailler-mattei, M. Elmansori, Effect of roughness scale on contact stiffness between solids, Wear 266 (2009) 589–591. http://dx.doi.org/10.1016/j.wear.2008.04.067.

[48] I. Demirci, S. Mezghani, M. Yousfi, M. El Mansori, Multiscale analysis of the roughness effect on lubricated rough contact, J. Tribol. 136 (2013) 011501. http://dx.doi.org/10.1115/1.4025222.

[49] I. Demirci, S. Mezghani, M. Yousfi, H. Zahouani, M. El Mansori, The scale effect of roughness on hydrodynamic contact friction, Tribol. Trans. 55 (2012) 705–712. http://dx.doi.org/10.1080/10402004.2012.694990.

[50] S.K. Chowdhury, A.D. Nimbarte, M. Jaridi, R.C. Creese, Discrete wavelet transform analysis of surface electromyography for the fatigue assessment of neck and shoulder muscles, J. Electromyogr. Kinesiol. 23 (2013) 995–1003. http://dx.doi.org/10.1016/j.jelekin.2013.05.001.

[51] X. Chen, J. Raja, S. Simanapalli, Multi-scale analysis of engineering surfaces, Int. J. Mach. Tools Manuf. 35 (1995) 231–238. http://dx.doi.org/10.1016/0890-6955(94)P2377-R.